Effective band structure of correlated materials: the case of VO_2

2007 J. Phys.: Condens. Matter 19 365206

(http://iopscience.iop.org/0953-8984/19/36/365206)

IOP PUBLISHING JOURNAL OF PHYSICS: CONDENSED MATTER

J. Phys.: Condens. Matter **19** (2007) 365206 (12pp) doi:10.1088/0953-8984/19/36/365206

Effective band structure of correlated materials: the case of VO_2

Jan M Tomczak and Silke Biermann

Centre de Physique Théorique, Ecole Polytechnique, 91128 Palaiseau Cedex, France

E-mail: jan.tomczak@cpht.polytechnique.fr

Received 20 December 2006
Published 24 August 2007
Online at stacks.iop.org/JPhysCM/19/365206

Abstract

Vanadium dioxide VO_2 and its metal–insulator transition at $T = 340$ K continue to receive considerable interest. The question whether the physics of the insulating low-temperature phase is dominated by the Mott or the Peierls scenario, i.e. by correlation or band effects, is still under debate. A recent cluster dynamical mean field theory calculation (Biermann *et al* 2005 *Phys. Rev. Lett.* **94** 026404) suggests a combination of both effects, characterizing the transition as of a correlation-assisted Peierls type. In this paper we present a detailed analysis of the excitation spectrum of the insulating M1 phase of VO_2, based on this calculation. We implement a scheme to analytically continue self-energies from Matsubara to real frequencies, and study the physics of the strong interactions, as well as the corresponding changes with respect to the density functional theory band structure within the local density approximation (LDA). We find that in the M1 phase lifetime effects are rather negligible, indeed allowing for an effective band structure description. A frequency-independent but orbital-dependent potential, constructed as an approximation to the full cluster dynamical mean field self-energy, turns out to satisfactorily reproduce the fully interacting one-particle spectrum, acting as a scissors operator which pushes the a_{1g} bonding and e_g^π bands apart and, thus, opens the gap.

(Some figures in this article are in colour only in the electronic version)

1. Introduction

One of the key issues of condensed matter physics, from both the theoretical and the experimental points of view, is the understanding of the electronic structure of materials. With the advent of density functional theory (DFT) within the local density approximation (LDA), or its gradient extensions, the *ab initio* calculation of electronic properties of astonishingly many classes of compounds became feasible in a reliable fashion [2]. The manageable complexity of the material is ever increasing and the verge of chemical precision is even coming into view.

From a conceptual point of view, however, this might appear rather miraculous, as there are severe, well-known, principle limitations. Indeed DFT is a theory of the ground state only. The interpretation of the Kohn–Sham eigenvalues of the effective one-particle system as excitation energies of the real N-particle system has no theoretical justification, and only the striking compatibility with experiment promotes this interpretation, which is often tacitly assumed.

On the other hand, regarding the original domain of the theory, i.e. ground-state properties, implementations of DFT inevitably have to resort to approximations, the exchange–correlation potential being unknown. This leads to the fact that, for some even apparently simple materials, the calculated ground state is found to contradict experimental findings. This is the case when electronic correlations, i.e. genuine many-body effects, invalidate the band picture which originates from an effective one-particle theory. The most prominent example is the Mott transition [3, 4], where the correlations prevail upon the itineracy of the electrons, forcing them to localize. Among the materials where this mechanism is present are for example Cr-doped V_2O_3 or the parent compounds of the high-T_c superconductors. A genuine signature of strong correlations, highly affecting the distribution of spectral weight, is the sensitivity to changes of external parameters, such as temperature or pressure, as is indeed observed in experiments such as transport, photoemission or optics.

The formidable task is to unravel the behaviour of a system in between these two limits: the effective free case (a problem that is diagonal in momentum space), and the atomic limit (that is diagonal in real space). In the latter, the notion of bands having lost its sense, the quantity to discuss is the spectral function. Within a band theory it will, for a given momentum, consist of Dirac distributions. With the increase of correlations these will broaden, due to scattering effects, inducing finite lifetimes, and lose weight that will reappear as incoherent features or satellites at different energies.

In this work, we present, for the specific example of the insulating phase of VO_2, a study of how correlations modify the excitation energies of the system and how, if at all, this can be cast into an effective one-particle picture.

To this effect, we implemented a scheme to analytically continue Matsubara self-energies to the real frequency axis, including for the first time the continuation of off-diagonal elements. This allows us to make a detailed analysis of recent cluster dynamical mean field calculations [1].

The paper is organized as follows. In section 2 we review the electronic structure of VO_2 and recent cluster dynamical mean field calculations. In section 3 we apply the analytical continuation scheme (that we detail in the appendix) and discuss the real-frequency self-energies for the M1 phase of VO_2. Section 4 presents a study of the correlation effects on the excitation spectrum and suggests an effective one-particle potential which corrects the LDA band structure.

2. Electronic structure of VO_2

2.1. Peierls versus Mott: a reminder

The phase diagram of vanadium dioxide, VO_2, intrigued condensed matter physicists for decades [5–13]. At high temperature, VO_2 is a (bad) metal and the crystal structure is of rutile type. At $T = 340$ K the compound undergoes a first-order metal–insulator transition (MIT) [14] and the structure becomes monoclinic (M1 phase). The paramount characteristic of the low-temperature structure is the pairing up of vanadium atoms, which form dimers along the c-axis that tilt out of the axis. Moreover, the phase is found to exhibit no local moment behaviour. There is a long-standing debate as to whether the MIT is primarily caused by

the structural change that doubles the unit cell (Peierls transition), or whether it is correlation effects that drive the system to become insulating (Mott–Hubbard transition).

VO_2 has a $3d^1$ configuration, and hence the key focus lies on the d-orbitals. The cubic component of the crystal field resulting from the octahedral coordination of the vanadium atoms in the rutile phase splits the d orbitals into an e_g and a t_{2g} manifold, the latter being lower in energy. The total crystal field further splits the t_{2g} into two e_g^π and a single a_{1g} orbital, which is directed along the *c*-axis. Both types of orbitals overlap, accounting for the metallic character of the rutile phase. In the M1 phase, where one has four formula units per unit cell, the a_{1g} orbitals split due to the dimerization into bonding/anti-bonding states. Furthermore, because of an increased hybridization with the oxygen 2p orbitals owing to the tilting of the dimers, the e_g^π are pushed up in energy relative to the former centre of the a_{1g} orbitals. Both these effects are working in favour of a gap opening [6]. However, LDA calculations, though decreasing the density of states at the Fermi level as compared to the rutile phase, fail to capture the experimental insulating gap (see figure 4), which is only opened once non-local correlation effects beyond the LDA are taken into account [1, 15, 16].

2.2. Dynamical mean field theory in a nutshell

A theoretical model, that embodies the above-mentioned struggle between localized and itinerant behaviour, or kinetic and potential energy, is the well-known Hubbard model. In the multi-band case its Hamiltonian reads

$$\mathbf{H} = \sum_{\mathbf{k},ll',\sigma} H_0^{ll'}(\mathbf{k}) c^\dagger_{\mathbf{k}l\sigma} c_{\mathbf{k}l'\sigma} + \sum_{\mathbf{R},ll',\sigma\sigma'}^{(l,\sigma)\neq(l',\sigma')} U_{ll'}^{\sigma\sigma'} n_{\mathbf{R}l\sigma} n_{\mathbf{R}l'\sigma'} \tag{1}$$

where $H_0^{ll'}(\mathbf{k})$ is the one-particle dispersion, l being an orbital index, and U an on-site Coulomb repulsion that is here limited to density–density terms only. $c^\dagger_{\mathbf{k}l\sigma}$, $c_{\mathbf{k}l\sigma}$ are the usual fermionic creation and annihilation operators and $n_{\mathbf{R}l\sigma}$ the corresponding number operators in real space. In a realistic context, the one-particle dispersion will be taken from e.g. an LDA calculation. Though the values of the interactions are often guided by constrained LDA [17], random phase approximation (RPA) [18] or experimental estimates, they remain parameters of the technique.

To solve this many-body problem in cases where the dominant correlation effects are local, a method of choice is the dynamical mean field theory (DMFT) and its realistic extension (LDA + DMFT) [4, 19]. The tremendous merit of DMFT is that it is a non-perturbative technique that is able to accurately describe the local physics, independent of the interaction strength. The dynamical aspect allows for an accurate description of spectral weight transfer to incoherent features.

The basic idea of DMFT is to replace a lattice problem (or as in the realistic case, a problem defined within a localized basis set) by an effective one-site system, coupled to a bath and subject to a self-consistency condition, analogously to conventional Weiss mean field theory in statistical mechanics. Contrary to the latter, however, the intervening mean field is energy dependent: hence the notion of a dynamical MFT. For solving the DMFT equations, a variety of techniques are available. In the case of realistic multi-band calculations, a widely used one is the quantum Monte Carlo (QMC). A common feature of QMC implementations is that they work within the finite-temperature Matsubara formalism, i.e. in imaginary time or frequency. Hence, an analytic continuation to the real frequency axis is needed. In the appendix we describe such a procedure for the DMFT self-energy in the most general case, that for the first time includes the continuation of off-diagonal elements. The scheme thus gives access to the full orbital physics, as well as to non-local (cluster DMFT) effects.

2.3. Recent DMFT results for VO_2

Recently, both the rutile and the M1 phase of VO_2 were investigated within DMFT [1, 16, 17]. Not surprisingly the insulating character of the monoclinic phase proved to be not capturable in the standard (single site) LDA + DMFT formalism without the unphysical creation of local moments. Instead, a cluster-extension of DMFT (CDMFT), where the solid is replaced not by a single impurity, but by a two-site cluster of vanadium atoms (surrounded by their oxygen octahedra) was needed [1]. It is of course very appealing, from the physical point of view, to choose the vanadium dimers as the fundamental unit of the calculation. Herewith non-local inter-vanadium correlations are treated in a non-perturbative manner. The calculation in [1] used an *N*MTO-Wannier Hamiltonian [20] where all orbitals other than the t_{2g} were downfolded, an on-site Coulomb repulsion $U = 4.0$ eV, a Hund's coupling $J = 0.68$ eV and a temperature $T = 770$ K. For solving the DMFT equations, the Hirsch–Fye quantum Monte Carlo (QMC) algorithm [21] was used. The insulating nature of the M1 phase is correctly described and the resulting local spectral functions of both phases compare favourably with photoemission and x-ray experiments [22–31]. The authors concluded that the non-local correlations effectively assist the Peierls-like transition, the dimerization leading to the formation of molecular singlets in the a_{1g} channel embedded in a bath.

3. The DMFT self-energy on the real frequency axis

3.1. Orbital structure of the self-energy

In the present work, we have implemented an analytic continuation procedure for imaginary frequency DMFT self-energies (see the appendix), which enabled us to develop a more detailed analysis of the above calculation. With the real-frequency self-energy at hand, interesting quantities become accessible, among which figure momentum-resolved spectral functions and linear response functions, such as the optical conductivity (when neglecting vertex corrections). In the following we shall analyse the correlation-induced modifications in the excitation spectrum of M1 VO_2 and discuss whether the result can still be cast into an effective band picture.

With four formula units in the unit cell, the M1 VO_2 self-energy matrix acquires the following form:

$$\Sigma_{\text{unitcell}} = \begin{pmatrix} \Sigma_{11} & \Sigma_{12} & 0 & 0 \\ \Sigma_{21} & \Sigma_{22} & 0 & 0 \\ 0 & 0 & \Sigma_{11} & \Sigma_{12} \\ 0 & 0 & \Sigma_{21} & \Sigma_{22} \end{pmatrix} \tag{2}$$

where the blocks Σ_{ij} are 3×3 matrices each, Σ_{ii} ($i = 1, 2$) are the local self-energy matrices for a given vanadium atom, and Σ_{12} and Σ_{21} are the inter-vanadium, intra-dimer blocks. Still, when given this additional freedom, the system is found to have in total only four non-equivalent self-energy elements. All other elements are zero within numerical precision. The self-energy for one dimer, i.e. the upper-left or lower-right 2×2 block in (2), comes out to be

$$\Sigma_{\text{dimer}} = \begin{pmatrix} \Sigma_{a_{1g}} & 0 & 0 & \Sigma_{a_{1g}-a_{1g}} & 0 & 0 \\ 0 & \Sigma_{e_g^\pi 1} & 0 & 0 & 0 & 0 \\ 0 & 0 & \Sigma_{e_g^\pi 2} & 0 & 0 & 0 \\ \Sigma_{a_{1g}-a_{1g}} & 0 & 0 & \Sigma_{a_{1g}} & 0 & 0 \\ 0 & 0 & 0 & 0 & \Sigma_{e_g^\pi 1} & 0 \\ 0 & 0 & 0 & 0 & 0 & \Sigma_{e_g^\pi 2} \end{pmatrix} \tag{3}$$

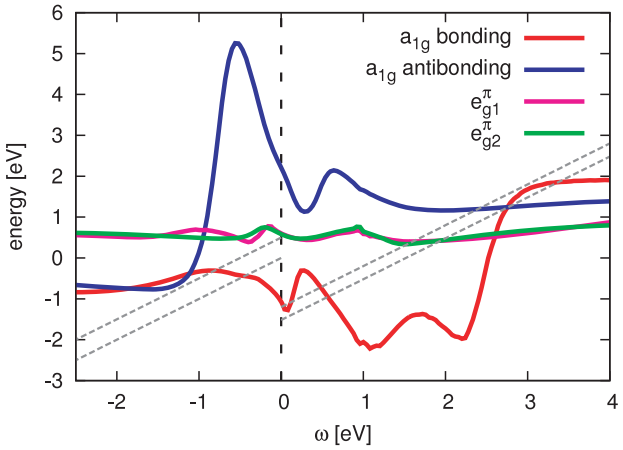

Figure 1. Real parts of the self-energy in the a_{1g} bonding/anti-bonding basis. The two stripes represent the position and bandwidth of the former LDA a_{1g} bonding ($\omega < 0$) and anti-bonding ($\omega > 0$) bands. See section 4.1.1 for a discussion.

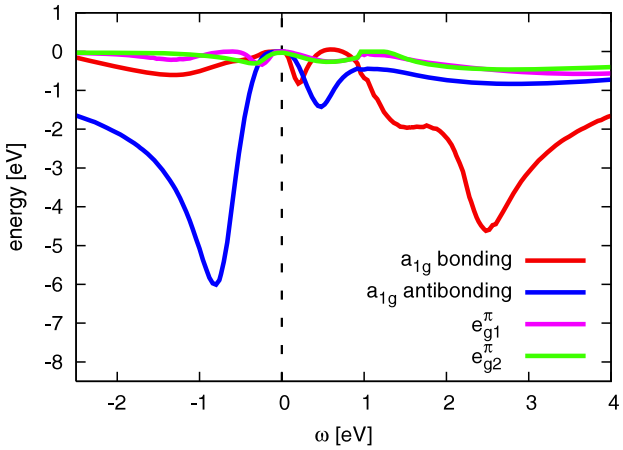

Figure 2. Imaginary parts of the CDMFT self-energy of the M1 phase of VO_2 in the a_{1g} bonding/anti-bonding basis. Note that all self-energy elements are regular at zero frequency. See section 3.2 for a discussion.

i.e. the intra-dimer coupling is entirely due to the a_{1g} channel, as can be expected from the discussed symmetry of the system.

3.2. Interpreting the self-energies: correlation effects in VO_2

Using the procedure detailed in the appendix, we compute the DMFT self-energies on the real frequency axis. Figures 1 and 2 display our result. We have chosen to change the basis of the a_{1g} components and to show their bonding/anti-bonding combinations $\Sigma_{b/ab} = \Sigma_{a_{1g}} \pm \Sigma_{a_{1g}-a_{1g}}$, in which the self-energy is diagonal in orbital space[1].

[1] We stress that this basis transformation can only be done *after* the DMFT calculation, as in this molecular picture the charges will no longer be centred on the atomic sites, and as a consequence local Hubbard–Hund Coulomb interaction terms would acquire an untractable form.

Several important observations can be made. The suppression of spectral weight at the Fermi energy can be achieved by two distinct behaviours of the imaginary parts of the self-energy within the charge gap. Either they diverge (as is the case of the insulating phase of the one-band Hubbard model), or they have to vanish within the gap. In the present case of M1 VO_2 we see in figure 2, that the self-energies are all regular and their imaginary parts vanish within the gap. Hence it is not a divergence of the effective mass that is responsible for the MIT.

Concerning the e_g^π elements, both the real and the imaginary part depend only weakly on frequency. Moreover, the imaginary part is globally low in magnitude, signalling only minor lifetime effects. This is a consequence of the low occupation of these orbitals ($\approx$16%). The interesting physics is carried by the a_{1g} components. They exhibit a rather selective dependence on frequency. The (anti)bonding component has a quite flat ((positive)negative) real and an unimportant imaginary part in the (un)occupied part of the spectrum. The d^1 configuration, with its nearly filled bonding bands, and empty anti-bonding bands, thus leads again—but this time in a non-trivial way—to only small lifetime effects. Despite the considerable on-site interactions, the complex structure of the self-energy thus suggests the existence of well-defined one-particle excitations. As we shall see below, this effective band structure is however strongly rearranged as compared to the former LDA energies, due to the differences in the regions of constant real-parts.

4. Effective band structures: at the rescue of the band-picture

4.1. The one-particle poles

When neglecting the anti-Hermitian parts of the self-energy, which—as we have seen above—are small for the bonding/anti-bonding bands, the excitation energies of the system are given by the poles of the one-particle Green's function:

$$\det(\omega_{\mathbf{k}} + \mu - H_0(\mathbf{k}) - \mathrm{Re}\,\Sigma(\omega_{\mathbf{k}})) = 0. \tag{4}$$

In contrast to the DFT equations, the above is not an eigenvalue problem, due to the frequency dependence of the self-energy. As a first step we shall discuss a graphical construction for finding solutions of (4).

4.1.1. One-particle excitations: a graphical construction. In the one-band case the problem reduces to $\omega_{\mathbf{k}} + \mu - \epsilon_{\mathbf{k}} - \mathrm{Re}\,\Sigma(\omega_{\mathbf{k}}) = 0$. Solutions are the intersections of the real part of the self-energy (minus μ) with a frequency stripe of slope one and a width corresponding to the dispersion of $\epsilon_{\mathbf{k}}$ bandwidth. In the general Hamiltonian case this construction is no longer exact, but it might still give qualitative insights. In the present case we expect this procedure to give a rather good description, when working in the bonding/anti-bonding basis and limiting ourselves to a discussion of the a_{1g} orbitals only. Indeed, if the e_g^π orbitals were empty, this construction would be exact.

In figure 1 we indicate the positions and bandwidths of the a_{1g} bands within the LDA. As in the bonding/anti-bonding basis the orbital pole equations approximately decouple, we show the LDA (anti-)bonding bandwidth only in the region ($\omega > 0$) $\omega < 0$, where relevant intersections can be found. Below the Fermi level, bonding pole solutions appear between -0.5 and -1.0 eV, due to intersections with the bonding part of the self-energy with the stripe representing the former LDA a_{1g} bonding band ($\omega < 0$). As a result, the bonding orbital is considerably pushed downwards in energy. The a_{1g} anti-bonding poles, i.e. the intersection of the anti-bonding self-energy and the stripe at $\omega > 0$ are pushed beyond 2 eV. Thus, already at this point, we suspect the spectral weight above 2 eV as seen in the local spectral function of [1] to stem from the a_{1g} anti-bonding excitation rather than an upper Hubbard band. We will come back to this point in the next section.

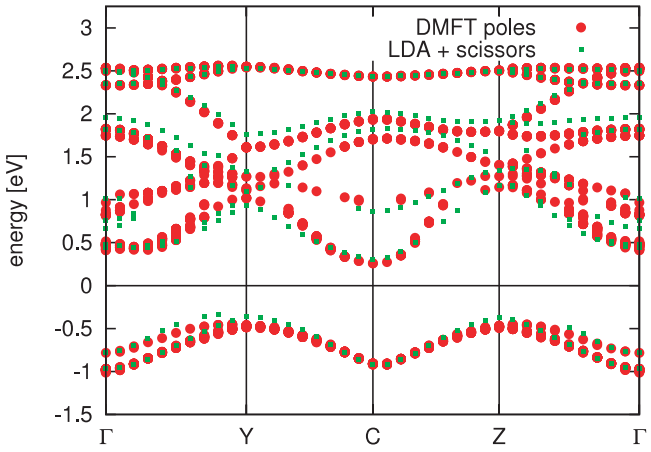

Figure 3. Comparison between the one-particle poles according to (4) and the bands using an optimized orbital-dependent but frequency-independent effective potential obtained as an approximation to the full CDMFT self-energies for various symmetry lines. See text for a discussion.

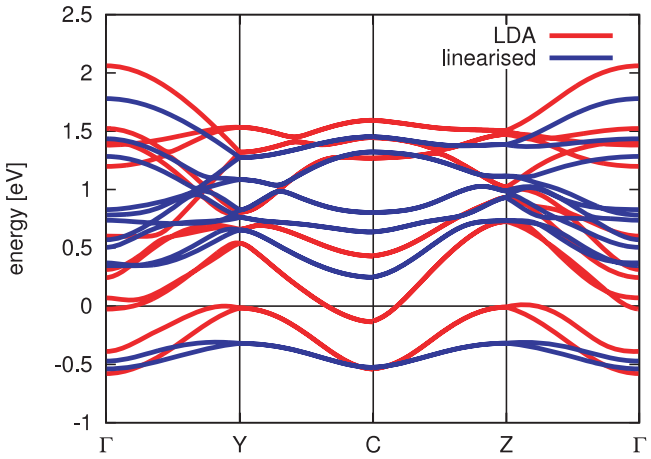

Figure 4. Comparison of the LDA bands with the bands resulting from the linearization scheme of (5).

4.1.2. One-particle excitations: poles of the Green's function. To solve the quasi-particle equation (4), one could in practice scan through frequency and look for sign changes of the determinant (4). However, as along various symmetry lines degenerate solutions exist, we had to introduce a threshold and solutions were identified as yielding an absolute value of the determinant below this value. Figure 3 shows our results.

On general grounds, there are, at a given **k**-vector, at least as many poles as there were LDA bands (including possible degeneracies). However, the frequency dependence of the self-energy may produce additional solutions for (4). In the particle–hole symmetric one-band Hubbard model, for example, there is one solution in the non-interacting limit, which simply is the one-particle dispersion, whereas in the atomic limit there are two poles at $\pm U/2$. In between there is a regime in which three poles may occur, representing the famous three-peak structure in the spectral function. In our example of the M1 phase of VO_2, we note that the

number of one-particle DMFT poles equals the number of LDA bands. In other words, the bands get shifted and reshaped, but the importance of incoherent features is rather small. This finding is far from trivial. For example, in the metallic rutile phase of VO_2 [31] or V_2O_3 [32], additional poles occur, representing incoherent Hubbard bands.

The most important changes as compared to the LDA is the opening of a gap between the bonding a_{1g} and the e_g^π bands. Besides, the anti-bonding a_{1g} band is shifted well beyond the e_g^π ones, as already seen in the graphical discussion above. In a molecular picture, the bonding/anti-bonding splitting of the a_{1g} orbitals, due to the dimerization, is tremendously enhanced by the *non-local* intra-dimer correlations that are caused by the *local* interactions. These results confirm the picture by Koethe *et al* who identify a high-frequency x-ray absorption spectroscopy (XAS) intensity peak as the a_{1g} anti-bonding band, while a small low-energy feature in the partial a_{1g} spectrum, seen both in the experiment and the CDMFT calculation, results from e_g^π–a_{1g} hybridization [30, 1].

The neglected lifetime effects will in our case broaden the spectra and shift the positions a little due to their frequency dependence, as can be seen in the (**k**-integrated) spectral function [1]. However, they will not, as is for example the case in V_2O_3 [32], completely suppress the spectral weight for some given pole solutions. Hence, in the current example, the effective band structure gives a quite accurate guidance to the physics of the system.

At first sight, it may seem surprising that despite strong local correlations—the imaginary parts of the on-site self-energies reach values of the order of 3 eV—well-defined one-particle excitations survive. Mathematically speaking, this is the consequence of a cancellation of local and inter-site self-energies resulting in nearly negligible lifetime effects for the (anti-)bonding bands at (positive)negative energies, respectively. Physically, enhanced inter-site hoppings allow the electrons to avoid the strong on-site repulsion by delocalizing over the dimer, and the resulting intra-dimer fluctuations reduce the net effects of the interaction.

4.2. Tailoring of a one-particle potential beyond the LDA: scissors at work

As we have seen, the frequency dependence of the bonding/anti-bonding self-energy in regions where they yield solutions of the pole equation is rather unimportant. Hence the question arises as to which extent one could derive the effective band structure from a constant one-particle, albeit orbital-dependent, potential Δ. To this end we will approximate our dynamical self-energy in a static way, by its values at the former LDA band-centres for the e_g^π and by the values at the pole energies for the a_{1g} orbitals. This means we choose $\Delta_{e_{g\,1}^\pi} = \mathrm{Re}\,\Sigma_{e_{g\,1}^\pi}(0.5\ \mathrm{eV}) - \mu = 0.48\ \mathrm{eV}$, $\Delta_{e_{g\,2}^\pi} = \mathrm{Re}\,\Sigma_{e_{g\,2}^\pi}(0.5\ \mathrm{eV}) - \mu = 0.54\ \mathrm{eV}$ for the e_g^π components, and $\Delta_b = \mathrm{Re}\,\Sigma_b(-0.75\ \mathrm{eV}) - \mu = -0.32\ \mathrm{eV}$, $\Delta_{ab} = \mathrm{Re}\,\Sigma_{ab}(2.5\ \mathrm{eV}) - \mu = 1.2\ \mathrm{eV}$ for the a_{1g} bonding/anti-bonding components respectively. As a consequence, there will be a downshift of the a_{1g} bonding band ($\Delta_b < 0$), which, together with an upshift of the e_g^π bands ($\Delta_{e_g^\pi} > 0$) is responsible for the opening of the gap. Thus, these considerations put numbers to Goodenough's picture [6]. However, the effect caused by the re-hybridizations with the oxygen bands, as described in section 1, is supplemented by the following. The correlations cause a depopulation of the e_g^π bands, in favour of the a_{1g} bonding one, as thereby the electrons are effectively avoiding the on-site Coulomb interaction. Moreover, the anti-bonding a_{1g} band is pushed up in energy way beyond all the e_g^π, tremendously enhancing the bonding/anti-bonding splitting.

After transforming back into the original basis, we solve the eigenvalue problem for $H_0(\mathbf{k}) + \Delta$. The results are shown in figure 3 along with the exact poles from above. The shiftings of the bands, owed to the additional potential, as described above, are, besides minor details, in excellent agreement with the CDMFT poles.

The above one-particle potential acts like a scissors operator and is somewhat reminiscent of results obtained within the GW approximation [33]. Indeed, within a model GW approach, a gap was found to open in the M1 phase [34]. Furthermore, preliminary results of a fully *ab initio* GW calculation [33] suggest that the GW approximation is as a matter of fact suited to describe the insulating character in the present case.

4.3. Linearizing the self-energy

Though disposing of the fully frequency-dependent DMFT self-energy, we find it instructive to compare with an approximate low-frequency expansion one would do if one had used a many-body technique that gives only information about the renormalization of low-lying coherent excitations, such as e.g. slave-boson theories. The renormalized band structure is then given by the solutions $\omega_{\mathbf{k}}$ of

$$\det\left(\omega_{\mathbf{k}} - Z\left[H_0(\mathbf{k}) + \mathrm{Re}\,\Sigma(\mathrm{i}\omega \to 0) - \mu\right]\right) = 0 \tag{5}$$

where $Z^{-1} = 1 - \partial_\omega \,\mathrm{Im}\,\Sigma(\mathrm{i}\omega)|_{\mathrm{i}\omega\to 0}$, and $(\mathrm{i}\,\mathrm{Im}\,\Sigma)\mathrm{Re}\,\Sigma$ is the (anti-)Hermitian part of the self-energy on the imaginary axis. This approach, exact at the Fermi level and normally identified with the Fermi liquid regime, may in principle be applicable in our case to the insulating phase of VO_2 since the self-energies do not diverge at low frequency, as is the case in the Mott insulating phase of the one-band Hubbard model. However, the quantity Z should, in this context, not be identified with the usual quasi-particle weight.

As can be seen in figure 4, a charge gap is found to open, thus correctly describing the insulating behaviour; however, when comparing to the one-particle poles, we notice huge discrepancies. The overall bandwidth is too small, the bands too flat and the bonding/anti-bonding splitting lacks the tremendous increase found before. This is natural, since foremost the involved slopes of the self-energy at low frequency overestimate the renormalizations towards the Fermi level, whereas at high enough energy the self-energies are essentially constant.

4.4. Conclusions

In conclusion, we have presented a detailed analysis of the excitation spectrum of the M1 phase of VO_2, with special emphasis on an effective band structure description. Indeed, we found lifetime effects to be rather negligible and the correlation effects to only shift and reshape the Kohn–Sham energies with respect to the starting LDA calculation. Furthermore, by approximating the dynamical self-energy, we were able to construct a frequency-independent, though orbital-dependent, one-particle potential that, when added to the LDA, reproduced the DMFT excitation energies to a quite satisfactory extent. We remark that due to the orbital dependence of this potential, it cannot be viewed as an improved density functional.

Hence, despite the undeniable presence of strong local correlations, the system retains the coherence of its excitations by means of intra-dimer fluctuations, to an extent that the physics of the compound is indeed dominated by the Goodenough–Peierls picture. The role of correlations consists in (i) pushing the a_{1g} anti-bonding band beyond the top of the e_g^π, consistent with the experimental findings, and, more importantly, in (ii) enhancing the a_{1g} bonding–e_g^π splitting due to an effectively reduced Coulomb repulsion in the a_{1g} bonding band, hence favouring the depopulation of the e_g^π bands. The latter results in the opening of the gap. Thus, as a matter of consequence it *is* the correlations that are responsible for the insulating state, albeit they cause it in a rather specific fashion.

Acknowledgments

We thank A I Poteryaev, A Georges and A I Lichtenstein for useful discussions and for collaborations which resulted in [1], which was the starting point for the present work. Furthermore, we appreciated discussions with F Aryasetiawan, M Gatti, L Reining, G A Sawatzky and A Tanaka. JMT kindly acknowledges support by the Japan Society for the Promotion of Science (JSPS) under grant PE05050. This work was supported by Idris, Orsay, under project no. 061393.

Appendix. Analytical continuation of the DMFT self-energy

Whereas for the continuation of the Green's function from the Matsubara formalism to real frequency a numerical approach, called the maximum entropy algorithm (MaxEnt) [35], has become a standard approach, the analytic continuation of the self-energy has only recently been envisioned in the context of realistic (i.e. multi-band) calculations [36–39].

In this work we have implemented a scheme that is sufficiently general to work in the multiorbital cluster DMFT case, and which, in particular, allows for off-diagonal self-energy elements. The following sketch outlines our continuation procedure:

$$\begin{aligned} &\text{QMC} : G_{ll'}(\tau) \\ &\qquad\downarrow \qquad\qquad\qquad \text{MaxEnt} \\ &A_{ll'}(\omega) = -1/\pi \,\mathrm{Im}\, G_{ll'}(\omega) \\ &\qquad\downarrow \qquad\qquad\qquad \text{Kramers–Kronig} \\ &G_{ll'}(\omega) = \sum_{k} [w + \mu - H_0(\mathbf{k}) - \Sigma(\omega + \mathrm{i}0^+)]^{-1}_{ll'} \\ &\qquad\downarrow \qquad\qquad\qquad \text{Root-finding} \\ &\Sigma_{ll'}(\omega) \end{aligned} \tag{A.1}$$

Starting from the local Green's function in imaginary time, we perform the aforementioned MaxEnt algorithm, yielding the spectral function, which is proportional to the imaginary part of the real-frequency Green's function. The real part of this quantity is related to the former by Kramers–Kronig transformation. By far the most difficult step in this scheme is the last one. Whereas in the one-band Hubbard model on the Bethe lattice an exact expression for the self-energy in terms of the Green's function exists ($\Sigma = \omega + \mu - t^2 G - 1/G$), in the general multi-band case a multi-dimensional root-finding procedure [40] has to be employed to solve (A.1). In the present case, of four formula units in the cell, the Hamiltonian is a 12×12 matrix and the self-energy has the structure shown in section 3.1.

In the degenerate case, the k-sum in (A.1) can be replaced by an integral over the density of states, and one ends up with the simpler task of inverting the Hilbert transform.

In the most general case, the starting Green's function will furthermore have off-diagonal elements in orbital space. As the standard implementation of the MaxEnt algorithm in this context has, to our knowledge, so far been used for diagonal elements only, some comments are in order. The equation that is to be inverted reads

$$G_{ll'}(\tau) = \int \mathrm{d}\omega \, A_{ll'}(\omega) K_\beta(\tau, \omega) \tag{A.2}$$

with $K_\beta(\tau, \omega)$ being the usual MaxEnt kernel [35].

In contrast to the diagonal elements of the spectral function, which are normalized to one and are positive at all frequencies, off-diagonal elements have vanishing zeroth moment and hence change sign as a function of ω.

For mending this difference, the idea is simply to add a function $f(\omega)$ of zeroth moment one to constant $A(\omega)$, and calculate the corresponding shift in $G(\tau)$. However, this function has to be chosen such that the resulting fictitious spectral function is non-negative for all frequencies. To this end, we construct it in the following way. Given the orthogonal orbital transformation $\tilde{A} = U^\dagger A_{ll'}$

$$U_{ll'} = \frac{1}{\sqrt{2}} \begin{array}{c} \\ \\ \\ \\ \\ \\ \end{array} \begin{array}{c} \begin{array}{cccccc} & & & \downarrow l' & & \end{array} \\ \begin{pmatrix} 1 & & -1 & & & \\ & \ddots & & & & \\ 1 & & 1 & & & \\ & & & \ddots & & \\ & & & & 1 & \end{pmatrix} \end{array} \begin{array}{l} \\ \\ \\ \leftarrow l \\ \\ \\ \end{array} \tag{A.3}$$

the ll-element ($l \lessgtr l'$) of the spectral function in the new basis reads

$$\widetilde{A}_{ll} = \frac{A_{ll} + A_{l'l'}}{2} \pm A_{ll'} \tag{A.4}$$

and is thus per construction a proper diagonal element of the spectral function in the rotated basis, i.e. in particular it is positive for all ω. Therefore $f = 1/2(A_{l'l'} + A_{ll})$ is a suitable shift for $\pm A_{ll'}$ in the original basis.

Hence, after having continued the original diagonal elements, one constructs as input the function

$$\widetilde{G}_{ll'}(\tau) = \left(U^\dagger G(\tau) U\right)_{ll'} = \int \mathrm{d}\omega\, \widetilde{A}_{ll'}(\omega) K_\beta(\tau, \omega) \tag{A.5}$$

from which, using (A.4), the off-diagonal spectral function is then deduced. We note that in the present case the above rotation has the same geometrical interpretation as the transformation into a bonding/anti-bonding basis, as used for the a_{1g} self-energies of VO_2, but the construction is more general and does not require special symmetry properties of the system.

References

[1] Biermann S, Poteryaev A, Lichtenstein A I and Georges A 2005 Dynamical singlets and correlation-assisted Peierls transition in VO_2 *Phys. Rev. Lett.* **94** 026404

[2] Jones R O and Gunnarsson O 1989 The density functional formalism, its applications and prospects *Rev. Mod. Phys.* **61** 689–746

[3] Imada M, Fujimori A and Tokura Y 1998 Metal–insulator transitions *Rev. Mod. Phys.* **70** 1039–263

[4] Georges A, Kotliar G, Krauth W and Rozenberg M J 1996 Dynamical mean-field theory of strongly correlated fermion systems and the limit of infinite dimensions *Rev. Mod. Phys.* **68** 13

[5] Zylbersztejn A and Mott N F 1975 Metal–insulator transition in vanadium dioxide *Phys. Rev.* B **11** 4383–95

[6] Goodenough J B 1971 The two components of the crystallographic transition in VO_2 *J. Solid State Chem.* **3** 490–500

[7] Wentzcovitch R M, Schulz W W and Allen P B 1994 VO_2: Peierls or Mott–Hubbard? A view from band theory *Phys. Rev. Lett.* **72** 3389–92

[8] Pouget J P, Launois H, Rice T M, Dernier P, Gossard A, Villeneuve G and Hagenmuller P 1974 Dimerization of a linear Heisenberg chain in the insulating phases of $V_{1-x}Cr_xO_2$ *Phys. Rev.* B **10** 1801–5

[9] Pouget J P, Launois H, D'Haenens J P, Merenda P and Rice T M 1975 Electron localization induced by uniaxial stress in pure VO_2 *Phys. Rev. Lett.* **35** 873–5

[10] Bulaevskii L N and Khomskii D I 1968 *Sov. Phys.—Solid State* **9** 2422

[11] Eyert V 2002 *Ann. Phys., Lpz.* **11** 650

[12] Korotin M A, Skorikov N A and Anisimov V I 2002 *Phys. Met. Metallogr.* **94** 17

[13] Tanaka A 2003 A new scenario on the metal–insulator transition in VO_2 *J. Phys. Soc. Japan* **72** 2433

[14] Morin F J 1959 Oxides which show a metal-to-insulator transition at the Neel temperature *Phys. Rev. Lett.* **3** 34–6

[15] Liebsch A, Ishida H and Bihlmayer G 2005 Coulomb correlations and orbital polarization in the metal–insulator transition of VO_2 *Phys. Rev.* B **71** 085109
[16] Laad M S, Craco L and Müller-Hartmann E 2006 Metal–insulator transition in rutile-based VO_2 *Phys. Rev.* B **73** 195120
[17] Anisimov V I, Zaanen J and Andersen O K 1991 Band theory and Mott insulators: Hubbard U instead of stoner I *Phys. Rev.* B **44** 943–54
[18] Aryasetiawan F, Imada M, Georges A, Kotliar G, Biermann S and Lichtenstein A I 2004 Frequency-dependent local interactions and low-energy effective models from electronic structure calculations *Phys. Rev.* B **70** 195104
[19] Kotliar G and Vollhardt D 2004 Strongly correlated materials: insights from dynamical mean-field theory *Phys. Today* **57** (3) 53
[20] Andersen O K and Saha-Dasgupta T 2000 Muffin-tin orbitals of arbitrary order *Phys. Rev.* B **62** R16219–22
[21] Hirsch J E and Fye R M 1986 Monte Carlo method for magnetic impurities in metals *Phys. Rev. Lett.* **56** 2521–4
[22] Shin S, Suga S, Taniguchi M, Fujisawa M, Kanzaki H, Fujimori A, Daimon H, Ueda Y, Kosuge K and Kachi S 1990 Vacuum-ultraviolet reflectance and photoemission study of the metal–insulator phase transitions in VO_2, V_6O_{13}, and V_2O_3 *Phys. Rev.* B **41** 4993–5009
[23] Goering E, Schramme M, Müller O, Barth R, Paulin H, Klemm M, denBoer M L and Horn S 1997 Leed and photoemission study of the stability of VO_2 surfaces *Phys. Rev.* B **55** 4225–30
[24] Kurmaev E Z, Cherkashenko V M, Yarmoshenko Yu M, Bartkowski St, Postnikov A V, Neumann M, Duda L C, Guo J H, Nordgren J, Perelyaev V A and Reichelt W 1998 Electronic structure of VO_2 studied by x-ray photoelectron and x-ray emission spectroscopies *J. Phys.: Condens. Matter* **10** 4081
[25] Sawatzky G A and Post D 1979 X-ray photoelectron and auger spectroscopy study of some vanadium oxides *Phys. Rev.* B **20** 1546–55
[26] Okazaki K, Wadati H, Fujimori A, Onoda M, Muraoka Y and Hiroi Z 2004 Photoemission study of the metal–insulator transition in VO_2/TiO_2 (001): evidence for strong electron–electron and electron–phonon interaction *Phys. Rev.* B **69** 165104
[27] Abbate M, de Groot F M F, Fuggle J C, Ma Y J, Chen C T, Sette F, Fujimori A, Ueda Y and Kosuge K 1991 Soft-x-ray-absorption studies of the electronic-structure changes through the VO_2 phase transition *Phys. Rev.* B **43** 7263–6
[28] Eguchi R, Taguchi M, Matsunami M, Horiba K, Yamamoto K, Ishida Y, Chainani A, Takata Y, Yabashi M, Miwa D, Nishino Y, Tamsaku K, Ishikawa T, Senba Y, Ohashi H, Muraoka Y, Hiroi Z and Shin S 2006 Evidence for a Mott-Hubbard metal-insulator transition in VO_2 *Preprint* cond-mat/0607712
[29] Haverkort M W, Hu Z, Tanaka A, Reichelt W, Streltsov S V, Korotin M A, Animisov V I, Hsieh H H, Lin H-J, Chen C T, Khomskii D I and Tjeng L H 2005 Orbital-assisted metal-insulator transition in VO_2 *Phys. Rev. Lett.* **95** 196404
[30] Koethe T C, Hu Z, Haverkort M W, Schussler-Langeheine C, Venturini F, Brookes N B, Tjernberg O, Reichelt W, Hsieh H H, Lin H-J, Chen C T and Tjeng L H 2006 Transfer of spectral weight and symmetry across the metal–insulator transition in VO_2 *Phys. Rev. Lett.* **97** 116402
[31] Tomczak J M, Aryasetiawan F and Biermann S 2007 submitted
[32] Poteryaev A I, Tomczak J M, Biermann S, Georges A, Lichtenstein A I, Rubtsov A N, Saha-Dasgupta T and Andersen O K 2007 *Preprint* cond-mat/0701263
[33] Hedin L 1965 New method for calculating the one-particle Green's function with application to the electron–gas problem *Phys. Rev.* A **139** A796–823
[34] Continenza A, Massidda S and Posternak M 1999 Self-energy corrections in VO_2 within a model GW scheme *Phys. Rev.* B **60** 15699–704
[35] Jarrell M and Gubernatis J E 1996 *Phys. Rep.* **269** 133
[36] Biermann S 2001 *Rep. Juelich Research Centre* p 3899
[37] Blümer N 2002 *PhD Thesis* Universität Augsburg
[38] Anisimov V I, Kondakov D E, Kozhevnikov A V, Nekrasov I A, Pchelkina Z V, Allen J W, Mo S-K, Kim H-D, Metcalf P, Suga S, Sekiyama A, Keller G, Leonov I, Ren X and Vollhardt D 2005 Full orbital calculation scheme for materials with strongly correlated electrons *Phys. Rev.* B **71** 125119
[39] Nekrasov I A, Held K, Keller G, Kondakov D E, Pruschke Th, Kollar M, Andersen O K, Anisimov V I and Vollhardt D 2006 Momentum-resolved spectral functions of $SrVO_3$ calculated by LDA + DMFT *Phys. Rev.* B **73** 155112
[40] Jarrell M, Freericks J K and Pruschke Th 1995 Optical conductivity of the infinite-dimensional Hubbard model *Phys. Rev.* B **51** 11704–11